Paleomass for R—bracketing body volume of marine vertebrates with 3D models (#87526)

First submission

Guidance from your Editor

Please submit by **17 Jul 2023** for the benefit of the authors (and your token reward) .

Structure and Criteria
Please read the 'Structure and Criteria' page for general guidance.

Raw data check
Review the raw data.

Image check
Check that figures and images have not been inappropriately manipulated.

If this article is published your review will be made public. You can choose whether to sign your review. If uploading a PDF please remove any identifiable information (if you want to remain anonymous).

Files

Download and review all files from the materials page.

6 Figure file(s)
1 Table file(s)

Structure and Criteria

Structure your review

The review form is divided into 5 sections. Please consider these when composing your review:

1. **BASIC REPORTING**
2. **EXPERIMENTAL DESIGN**
3. **VALIDITY OF THE FINDINGS**
4. General comments
5. Confidential notes to the editor

📄 You can also annotate this PDF and upload it as part of your review

When ready [submit online](#).

Editorial Criteria

Use these criteria points to structure your review. The full detailed editorial criteria is on your [guidance page](#).

BASIC REPORTING

- Clear, unambiguous, professional English language used throughout.
- Intro & background to show context. Literature well referenced & relevant.
- Structure conforms to [PeerJ standards](#), discipline norm, or improved for clarity.
- Figures are relevant, high quality, well labelled & described.
- Raw data supplied (see [PeerJ policy](#)).

EXPERIMENTAL DESIGN

- Original primary research within [Scope of the journal](#).
- Research question well defined, relevant & meaningful. It is stated how the research fills an identified knowledge gap.
- Rigorous investigation performed to a high technical & ethical standard.
- Methods described with sufficient detail & information to replicate.

VALIDITY OF THE FINDINGS

- ℹ️ Impact and novelty not assessed. *Meaningful* replication encouraged where rationale & benefit to literature is clearly stated.
- All underlying data have been provided; they are robust, statistically sound, & controlled.
- Conclusions are well stated, linked to original research question & limited to supporting results.

Standout reviewing tips

The best reviewers use these techniques

Tip	*Example*
Support criticisms with evidence from the text or from other sources	*Smith et al (J of Methodology, 2005, V3, pp 123) have shown that the analysis you use in Lines 241-250 is not the most appropriate for this situation. Please explain why you used this method.*
Give specific suggestions on how to improve the manuscript	*Your introduction needs more detail. I suggest that you improve the description at lines 57- 86 to provide more justification for your study (specifically, you should expand upon the knowledge gap being filled).*
Comment on language and grammar issues	*The English language should be improved to ensure that an international audience can clearly understand your text. Some examples where the language could be improved include lines 23, 77, 121, 128 – the current phrasing makes comprehension difficult. I suggest you have a colleague who is proficient in English and familiar with the subject matter review your manuscript, or contact a professional editing service.*
Organize by importance of the issues, and number your points	*1. Your most important issue* *2. The next most important item* *3. ...* *4. The least important points*
Please provide constructive criticism, and avoid personal opinions	*I thank you for providing the raw data, however your supplemental files need more descriptive metadata identifiers to be useful to future readers. Although your results are compelling, the data analysis should be improved in the following ways: AA, BB, CC*
Comment on strengths (as well as weaknesses) of the manuscript	*I commend the authors for their extensive data set, compiled over many years of detailed fieldwork. In addition, the manuscript is clearly written in professional, unambiguous language. If there is a weakness, it is in the statistical analysis (as I have noted above) which should be improved upon before Acceptance.*

Paleomass for R—bracketing body volume of marine vertebrates with 3D models

Ryosuke Motani [Corresp. 1]

[1] Departement of Earth and Planetary Sciences, University of California, Davis, Davis, California, United States of America

Corresponding Author: Ryosuke Motani
Email address: rmotani@ucdavis.edu

Body mass is arguably the most important characteristic of an organism, yet it is often not available in biological samples that have been skeletonized, liquid-preserved, or fossilized. The lack of information is especially problematic for fossil species, for which individuals with body mass information are not available anywhere. Multiple methods are available for estimating the body mass of fossil terrestrial vertebrates but those for their marine counterparts are limited. Paleomass is a software tool for estimating the body mass of marine vertebrates from their orthogonal silhouettes through bracketing. It generates a set of two 3D models from these silhouettes, assuming superelliptical body cross-sections with different exponent values. By setting the exponents appropriately, it is possible to bracket the true volume of the animal between those of the two models. The original version phased out together with the language platform it used. A new version is reported here as an open-source package based on the R scripting language. It inherits the underlying principles of the original version but has been completely rewritten with a new architecture. For example, it first produces 3D mesh models of the animal and then measures their volumes and areas with the VCG library, unlike the original version that did not produce a 3D model but instead computed the volume and area segment by segment using parametric equations. The new version also exports 3D models in polygon meshes, allowing later tests by other software. Other improvements include the use of NACA foil sections for hydrofoils such as flippers, and optional interpolation with local regression. The software has a high accuracy, with the mean absolute errors of 1.33% when the silhouettes of the animals are known.

1 # Paleomass for R—bracketing body
2 # volume of marine vertebrates with 3D
3 # models

4
5
6 Ryosuke Motani[1]

7

8 [1] Department of Earth and Planetary Science, University of California, Davis, California, U.S.A.

9
10 Corresponding Author:
11 Ryosuke Motani[1]
12 Email address: rmotani@ucdavis.edu
13
14

Abstract

Body mass is arguably the most important characteristic of an organism, yet it is often not available in biological samples that have been skeletonized, liquid-preserved, or fossilized. The lack of information is especially problematic for fossil species, for which individuals with body mass information are not available anywhere. Multiple methods are available for estimating the body mass of fossil terrestrial vertebrates but those for their marine counterparts are limited. Paleomass is a software tool for estimating the body mass of marine vertebrates from their orthogonal silhouettes through bracketing. It generates a set of two 3D models from these silhouettes, assuming superelliptical body cross-sections with different exponent values. By setting the exponents appropriately, it is possible to bracket the true volume of the animal between those of the two models. The original version phased out together with the language platform it used. A new version is reported here as an open-source package based on the R scripting language. It inherits the underlying principles of the original version but has been completely rewritten with a new architecture. For example, it first produces 3D mesh models of the animal and then measures their volumes and areas with the VCG library, unlike the original version that did not produce a 3D model but instead computed the volume and area segment by segment using parametric equations. The new version also exports 3D models in polygon meshes, allowing later tests by other software. Other improvements include the use of NACA foil sections for hydrofoils such as flippers, and optional interpolation with local regression. The software has a high accuracy, with the mean absolute errors of 1.33% when the silhouettes of the animals are known.

Introduction

Body mass is an essential metric to describe aspects of the biology of individual organisms (Schmidt-Nielsen, 1984). Despite the importance, a body mass record is not always available — preserved specimens in museum collections often lack body mass information, and fossil organisms are never found with body mass data. The lack of information is not overly problematic for extant species for which conspecific individuals are available elsewhere, but poses a critical hurdle to biological studies of fossil species. Accordingly, paleontologists have been exploring the possibility of body mass estimation based on what is preserved in fossils.

Methods for body mass estimation based on fossils are largely divided into two categories depending on the underlying principle—one may be called the length-based and the other volumetric approaches (Hurlburt, 1999; Smith, 2002; Sellers et al., 2012). The length-based approach first establishes a correlation between the length(s) of one or more morphological character(s) of the animals in question and their body mass through a linear regression, based on extant samples for which the body mass is known, and then uses the regression equation to estimate the body mass of extinct animals for which the length character(s) are available. Multiple regression with more than one length characters tends to be

52 preferred in clades in which fossils species are nested among abundant extant members, such as
53 mammals (e.g., Smith, 2002; Mendoza, Janis & Palmqvist, 2006), whereas bivariate regression is
54 almost exclusively used in clades that have long been extinct with only distantly related
55 descendants surviving, e.g., non-avialan dinosaur clades (Anderson, Hall‐Martin & Russell,
56 1985; Campione & Evans, 2012), probably to avoid overfitting of the model to particular extant
57 clades that would mislead the outcome.
58   The volumetric approach first estimates the volume of the animal in question and then
59 converts the value to body mass by assuming an average body density. This approach dates back
60 at least to 1905, when the body mass of *Brontosaurus* was estimated by measuring the volume of
61 a cast of a scaled physical model with water displacement and then converting the volume to
62 mass by assuming the freshwater density (Gregory, 1905). A similar method was used by
63 (Colbert, 1962) for body mass estimation of ~~broader~~ dinosaurs. As mathematical models became
64 common, a parametric approach to model the body as a collection of cylinders based on a limited
65 number of measurements, called Graphic Double Integration, was developed (Jerison, 1973).
66 What may be considered an extension of this approach, where the body is straightened in a
67 parametric space and modeled by many cylindrical disks, was later proposed (Seebacher, 2001).
68 With the arrival of 3D computer technology, methods of incorporating complex 3D computer
69 models emerged. Such methods include a partly parametric approach as in Paleomass based on
70 superelliptical cross-sections (Motani, 2001), as well as the minimum convex hull method based
71 on completely empirical data from laser scanning of mounted skeletons (Sellers et al., 2012).
72   These methods aim to arrive at the best mean estimate of body mass, except Paleomass
73 which tried to bracket the mass between two values (Fig. 1D bracketed by C and E). The method
74 was also unique for specifically addressing marine vertebrates, for which a limb-based regression
75 approach is not suitable because they do not support the body mass with the limbs. Despite the
76 uniqueness that would allow cross-checking of other methods, the software is no longer available
77 because its language platform was discontinued. The purpose of the present paper is to report a
78 completely rewritten and open-source version of Paleomass with a new architecture and
79 enhancements over the original version.

Materials & Methods

Platform

82 The new Paleomass was written in the R scripting language and run on the R platform (R-Core-
83 Team, 2020). Apart from the default R packages, it relies on the following packages for parts of
84 computation: imager (Barthelmé & Tschumperlé, 2019), locfit (Loader, 1999), Morpho
85 (Schlager, 2017), plot3D (Soetaert, 2022), rgl (Murdoch, 2001), and Rvcg (Schlager, 2017). It is
86 open-source and provided under GNU General Public License v3.0. A repository for the
87 package, including the code and a tutorial, is found at: https://github.com/rmotani/paleomass.

Aim

Paleomass aims to estimate the body volume of a marine vertebrate with a straight body axis. The volume is converted to a mass by assuming the average body density that can be specified by the user. The body surface area is also estimated simultaneously.

Principle

Paleomass aims to bracket the true body volume of a marine vertebrate between those of two 3D models (Fig. 1). Each of the two models is not the best mean estimate of the true body shape, but one is expected to have a volume slightly larger than the true body volume (Fig. 1E versus D), and the other slightly smaller (Fig. 1C). The models are based on the same set of orthogonal body silhouette images and therefore appear identical in completely dorso-ventral or lateral views, but have different cross-sectional shapes and differs in coronal view.

The cross-sectional shape is based on superellipses (Fig. 1A), which are mathematical expansions of ellipses. Whereas ellipses are defined as:

$$(x/a)^2 + (y/b)^2 = 1$$

superellipses are defined by an equation:

$$|x/a|^n + |y/b|^n = 1 \tag{1}$$

where $n > 0$. When $n = 2$, a superellipse becomes an ellipse (Fig. 1). As n decreases from 2, the superellipse approaches a diamond shape as n approaches 1 and then a cross shape as it approaches 0. If n increases beyond 2, the superellipse approaches a rectangle.

It is known that a typical body cross-section of a ~~marine~~ vertebrate can be approximated by a superellipse or a combination of two halves of different superellipses (Motani, 2001). The true body cross-sections of marine tetrapods are usually found to be bracketed by two superellipses, one with $n = 2$ and the other with $n = 3$ (but see Validation below for a narrower range). For fish, the two exponents are $n = 1.5$ and 2.5. Therefore, the true volume of a marine vertebrate can be bracketed by making two 3D models with these two boundary superelliptical shapes, depending on the clade (Fig. 1).

Overall workflow

Paleomass first reads in the data from raster images and command line options, based on which it computes 3D mesh models for the main body and each of the fins and flippers separately. Two mesh models are made for the main body, with different superelliptical exponents of choice. The volume and surface area of each mesh model are computed and summed to give two total estimates, with different main body models. Optionally, these meshes are assembled to make a complete 3D mesh model. The assembled models and each part model can be saved as 3D polygon meshes, respectively.

Coordinate system

Modeling and computation take place in a three-dimensional Euclidean coordinate system. The x axis is set as the bilateral axis with the right side of the body being the positive side. The y axis is the dorsoventral axis with the dorsal direction being positive, while the z axis is the antero-posterior axis, which may also be called the body axis hereafter, with the tip of the snout being the origin and the posterior direction being positive.

User supplied data

The users need to supply the shape and size of the animal to be modeled. First, the shape is supplied as a set of silhouette raster images, such as JPEG or PNG, one for each fin/flipper/cephalofoil and a pair for the body (e.g., Fig. 2C). These images need to have the same pixel size, e.g., if each side of pixel is 0.001 m in one image, then this pixel side length should be the same in all other images. It is recommended to have at least 3000 pixels along the body axis of these images (see Validation below), rather than 1000 as originally suggested (Motani, 2001). The body images are in lateral and dorsoventral views, respectively, with all fins, flippers and cephalofoils removed. For each fin, flipper, and cephalofoil, a planar view is required. Second, the length of the body axis as represented in the body images after the removal of the fin/flipper/cephalofoil is supplied through a command line option, in meters.

Paleomass accepts the following types of fins and flippers: pectoral fin/flipper, pelvic fin/flipper, caudal fin, dorsal fin, second dorsal fin, and anal fin. Not all fins/flippers have to be present. This versatility allows for different body architectures to be modelled (Fig. 4).

Computation steps for main body

The computation of a 3D model and its volume for the main body follows the steps below.
(1) The lateral and dorso-ventral silhouettes of the main body of the animal in question are read from raster image files (Fig. 3A, B).
(2) The outlines of these silhouettes are digitized as coordinates (Fig. 3C, D), which are then optionally smoothed through interpolation with local regression using the locfit() function (Loader, 1999). By default, a nearest neighbor parameter of 0.1 and a constant component of 0 is used for local regression but the former value is user adjustable. The smoothing allows coordinates to take non-integer values and therefore prevents step-like appearance of the final 3D model (Fig. 3G, H) that often gives rise to non-manifold edges and triangles that cause errors later on.
(3) The transverse and dorsoventral diameters of the main body are calculated from the coordinates for each pixel position along the body axis (Fig. 3C, D). There are much less than 3000 lines in Fig. 3C and D for visualization purposes but the actual calculations are done for each pixel point along the body axis, i.e., there would be 3000 pairs of transverse and dorsoventral diameters in the input body images have 3000 pixels along the body axis.

158   (4) Based on these coordinates and diameters, a superellipse is drawn per segment (Fig. 3E, F),

159   i.e., body mages with 3000 pixels along the body axis will result in 3000 superellipses. Each

160   superellipse has 181 vertices around its perimeter so that there is one vertex per every 2° of

161   angular displacement around the center, with the first and last vertices overlapping—these two

162   vertices will be merged later to make the model watertight, reducing the number of vertices per

163   segment to 180. The number of vertices per segment is user adjustable. The exponent for the

164   superellipse (n in equation 1) is also set by the user, e.g., 2 for one model (e.g., Fig. 3E) and 2.4

165   for the other (Fig. 3F) for marine tetrapods.

166   (5) A tip is added at each of the anterior and posterior ends of the body to help make the model

167   watertight at a later stage. These tips are small superelliptical disks with a tiny radius of 10^{-4}

168   pixels. They do not affect the computation of volume and surface area. The radius of the tip is

169   user adjustable.

170   (6) Superellipses from steps 4 and 5 are connected as a 3D mesh (Fig. 3G-J).

171   (7) Small holes at the tips of the body are closed by merging closely located vertices within

172   distances of 10^{-4} pixels or less, and then the whole mesh is cleaned for duplicate faces and non-

173   manifold faces and vertices by vcgClean() function (Schlager, 2017). Cleaning may fail if

174   smoothing is skipped at step 2, leaving non-manifold edges that would prevent accurate volume

175   calculation. Also, sticky non-manifold edges may result from having low-resolution input

176   images—having 3000 rather than 1000 pixels are necessary along the body axis ~~would~~ help

177   prevent this unintended error.

178   (8) The volume and surface area of the model are measured by vcgVolume() and vcgArea(),

179   respectively (Schlager, 2017). Initially, they are calculated in cubic pixels and square pixels,

180   respectively, where pixel size is as in the input images. These values are then converted to m^3

181   and m^2s using the body axis length provided by the user, in combination with the number of

182   pixels along the body axis in the input images.

Computation steps for fins and flippers

184   The computation of a 3D model and its volume for a fin or flipper follows the steps below.

185   (1) The planar image of a fin is read from a raster image (Fig. 3K).

186   (2) The outline of the image is digitized as coordinates (Fig. 3L), and smoothing through local

187   regression is applied as in the main body outline. The default nearest neighbor parameter for

188   local regression is 0.1 but Fig. 3O was produced with a value of 0.05.

189   (3) NACA 4-digit foil section is drawn at each pixel point along the span of the fin (Fig. 3M).

190   Symmetrical sections without a camber are used. The equation for such a section is given by:

191            $y = 5t[0.2969x^{0.5} - 0.126x - 0.3516x^2 + 0.2843x^3 - 0.1015x^4]$

192   where x is the position along the chord given as a fraction between 0 and 1, and t is the thickness

193   of the foil relative to the chord in percentages (Ladson & Brooks, 1975). The base value of t is

194   set at 10 for the anal and second dorsal fins and 20 for the rest—these values are user adjustable.

195   When using the base thickness to construct a fin, the thickness distribution along the span

196   becomes proportional to the chord length distribution and thus results in a strange shape. Most

197 importantly, the part of the fin that is supposed to be thickest along the fin span, e.g., proximal
198 end of the pectoral fin/flipper, is not always reconstructed with the maximum thickness. To avoid
199 this, the base thickness is scaled by a thickness envelope calculated with the following steps.
200 First, the point along the span where the maximum thickness is expected is specified as a fraction
201 between 0 and 1. For example, this point would be 0 for pectoral fin/flipper and 0.5 for a
202 symmetric caudal fin. Second, the axis from the thickest point to an end of the fin span is given
203 new coordinates of 1 to 0, with 1 at the thickest point 0 at the distal tip. Lastly, the square roots
204 of these values are calculated to form the thickness envelope to scale the raw thickness based on
205 the chord lengths. For example, at the midpoint between the thickest point and a fin tip, the raw
206 thickness is multiplied by $0.5^{0.5}$. to give a scaled thickness. This scaling was not present in the
207 original Paleomass.
208 (4) Foil sections from the previous step are connected to produce a 3D mesh (Fig. 3N, O), which
209 are then cleaned as in the body mesh.
210 (5) The volume and surface areas are measured as in the body mesh.
211 (6) The processes above are repeated for all fins/flippers.

Computation of cephalofoil

213 A simple cephalofoil model is implemented to accommodate hammerhead sharks. A cephalofoil
214 mesh is built in the same manner as fins and flippers, in that serial NACA foil sections are used.
215 However, unlike fins and flippers that gradually thin out toward the tip, the two ends of the
216 cephalofoil, where the eye sockets are located, are thickened.

Body and fin integration

218 This process is for visualization purposes only at present and does not affect the volume/area
219 estimation. Paleomass allows adjustment of the position and angle of each fin/flipper relative to
220 the main body through command line options. Specifically, positioning along the x, y, and z
221 axes, as well as rotation around these three axes can be adjusted. Rotations are called pitch, yaw,
222 and roll, around the x, y, and z axes, respectively. Roll is applied first, followed by pitch, and
223 then yaw.

Mass calculation

225 Once the volume of each component is estimated, they are summed to give a total volume. If
226 there is overlap among components, then the overlapping part is counted twice. However, such
227 overlap is usually limited compared to the body volume and would not cause a significant error
228 as evident from the validation results given later. It is ideal to find a Boolean union of 3D meshes
229 but such a function is not yet stably available in R. Future development may allow addition of a
230 Boolean union procedure.

231   With the total volume estimated, body mass is calculated from the volume by assuming a
232 mean density of the total body. For marine vertebrates with buoyancy control through an air
233 bladder or lungs, it is expected that neutral buoyancy is experienced in at least a part of daily life.
234 The neutral buoyancy near the sea surface would suggest a mean body density of 1.027 g/cm^3,
235 and that in pure water is approximately 1 g/cm^3 (Stewart, 2008). By default, Paleomass uses
236 these two values, although one of them is user adjustable.
237   The total body density of vertebrates has been controversial. Colbert (1962) used 0.9
238 g/cm^3 based on a value from *Alligator mississippiensis*—however, alligators are capable of being
239 suspended in freshwater, i.e., their mean density could become about 1 g/cm^3 depending on how
240 much air is in the lung. Sellers et al. (2012) used a value of 0.896 g/cm^3, which they calculated
241 based on a dataset from a frozen horse reported by Buchner et al. (1997). However, a
242 reexamination of this dataset suggests that the value should be 0.915 g/cm^3–0.896 would be
243 derived instead if the limbs from only one side of the body are included in calculation. This last
244 value of 0.915 is almost identical to the density of ice, so freezing of the specimen may have
245 biased the data, i.e., the true value may be close to 1 without freezing. The total body density of
246 sharks in Florida varied between 1.02 and 1.07 g/cm^3 (Baldridge, 1970), whereas the same in rat
247 varied between 1.03 and 1.09 g/cm^3 depending on the body fat content (Dahms & Glass, 1982).
248 Overall, freshwater or seawater density still remains the most reasonable value, especially for
249 marine vertebrates.

Validation

251 The accuracy of the software was tested in two ways. First, its accuracy under the best condition
252 was tested by geometric objects of known volume and area, a sphere and prolate spheroid.
253 Second, its ability to bracket the true volume and surface area of actual aquatic vertebrates was
254 tested. In both tests, Paleomass was used with interpolation with local regression enabled.

Geometric objects

256   The first test followed the steps below. A circle and an ellipse were drawn in CorelDraw
257 and exported as raster images, respectively, so that the long axis of the object varies from 100 to
258 10000 pixels, with an increment of 100 between 100 and 1000, and 1000 between 1000 and
259 10000. Then, the volumes of spheres and prolate spheroids based on these images were estimated
260 by using each image as both the lateral and dorso-ventral views for the body in Paleomass, per
261 run. The estimated values were then compared to the true values from parametric equations
262 describing the volume and surface area of spheres and prolate spheroids. The result shows that
263 the error is less than 0.5% in both volume and surface area estimation as long as the resolution of
264 the input image is high, with at least about 800 pixels along the long axis (Fig. 5). However, to
265 stably obtain best results, it is recommended to have 3000 or more pixels along the body axis

266 (Fig. 5B). Such a high resolution is also beneficial in minimizing unintended production of non-
267 manifold edges as mentioned earlier.

268 3D models of actual animals

269   The second test is based on 3D mesh models of 25 marine vertebrate species, digitized
270 from actual animals. Only those 3D models that were produced in association with universities
271 (Kano et al., 2013; Irschick et al., 2021) were used. The species include 20 osteichthyes, 3
272 chondrichthyes, and 2 cetaceans—the list of species used is given in supplementary information.
273 The uneven distribution across clades reflects biased data availability that cannot be easily
274 amended.
275   First, the true volume and surface area of each animal were recorded, after making its 3D
276 model watertight in Meshlab (Cignoni et al., 2008). This involved removal of duplicate vertices
277 and faces, followed by an iteration of a sequence comprising deletion of non-manifold edges and
278 self-intersections and filling of the resulting holes. If error-causing borders remained after the
279 iteration, the borders were removed and the iteration sequence was reinitiated. Second,
280 Paleomass estimates of the volume and surface area were calculated based on the lateral and
281 dorso-ventral images of the model, which were captured under orthographic projection in
282 Meshlab (Fig. 2A), together with images from angles that reveal the planar views of individual
283 fins/flippers (Fig. 2B). Attention was paid not to change the magnification between image
284 captures. These images were edited in CorelDraw to separate fins/flippers from the body and
285 then each part was saved as a raster image (Fig. 2C). The image resolution was set so that there
286 are 3000 pixels along the long axis of the main body. Paleomass estimates were made for
287 superelliptical exponents (n in equation 1) from 1.5 to 3.0 by an increment of 0.1. Finally, the
288 Paleomass estimates were compared to the true values to test if the latter were bracketed by any
289 pair of the Paleomass estimates.
290   The results are summarized in Fig. 6. In all cases, the true volumes of the marine
291 vertebrates were found to be bracketed between Paleomass estimates with superelliptical
292 exponent values of 1.6 and 2.4. Within this range, cohorts are recognized based on how round
293 the ventral half of the body coronal sections are—some species have rounded ventral halves that
294 appear U-shaped (e.g., Fig. 6E) and found toward the right side of the plot, whereas others have
295 sharper ventral halves appearing closer to a V-shape (e.g., Fig. 6C) and located toward the left
296 side. In sharks, this is upside down, i.e., it is the shape of the dorsal halves that may be rounded
297 or Λ-shaped (Fig. 6A). Most osteichthyes in the data have intermediate ventral halves between
298 V- and U-shape (e.g., Fig. 6D) and consequently found in a moderate exponent range of 1.8 to
299 2.1. However, unusual forms are found outside of this typical range—those with flattened ventral
300 sides, such as pufferfish and eels, are in the range of 2.2 to 2.4, whereas those with exceptionally
301 compressed cross-sections with V-shaped ventral halves, such as flatfish and small herring, are
302 in the range of 1.6 to 1.7. Cetaceans, with their coronal sections rounded ventrally, have a high
303 optimal exponent range of 2.0 to 2.3. Sharks tend to have Λ-shaped dorsal halves but this is

304   partly compensated for by the flat ventral halves, resulting in a moderate exponent range of 1.8
305   to 2.0. The optimal exponent range for the surface area was between 1.6 and 2, when excluding
306   unusual forms such as flatfish and pufferfish. These optimal ranges mostly overlap the
307   previously suggested ranges (Motani, 2001) while being narrower and better defined.
308   The accuracy of Paleomass estimates was computed in the following manner. Paleomass
309   provides a range of estimates rather than a single mean estimate, while the latter would be
310   required to compute accuracy. Therefore, the mean of the upper and lower bounds of the
311   estimated volume range was used as a single estimate of the volume to facilitate error
312   calculation. With this treatment, the mean and maximum absolute estimation errors are 1.33 and
313   3.15% across 25 species, using the cohort-specific superelliptical exponent ranges of 2.0-2.3 for
314   cetaceans, 1.8-2.0 for sharks, 1.8-2.1 for typical fish, 2.2-2.4 for U-shaped fish, and 1.6-1.7 for
315   V-shaped fish. When applying the more inclusive exponent range of 1.6-2.4 to all species, the
316   errors increase to 4.61 and 7.21%, respectively. For the surface area, the mean and maximum
317   absolute error are 2.64 and 10.5%, respectively, when using the same inclusive range of 1.6-2.4.

Discussion

318

319   The validation results suggest that Paleomass successfully brackets the true volume and surface
320   area of marine vertebrates when the body silhouettes are known—the software has high
321   accuracy, with a mean absolute error of 1.33%. At the same time, there are limitations to the
322   software package. Paleomass is designed for marine vertebrates with straight body axis and
323   cannot manage lateral concavities in body shape or dorso-ventral concavities in fins/flippers.
324   Also, as stated earlier, the software lacks the capability for Boolean union of body part meshes
325   until such becomes stably available in R. Finally, the accuracy of body mass estimates depends
326   on that of the body outline images, as well as the choice of superelliptical exponent and mean
327   body density.
328   The accuracy of body outline information merits a discussion. There is a paucity of body
329   outline information in the fossil record in general: some fossil species, such as the ichthyosaur
330   *Stenopterygius* and *Aegirosaurus* (Motani, 2005; Delsett et al., 2022), are occasionally preserved
331   with body outlines but the majority of species lack such information. For species without body
332   outlines preserved, outlines are often drawn around the skeleton, usually without strict accuracy
333   control. Therefore, the accuracy of body mass estimation for those fossil vertebrates would be
334   lower than that of the software itself because of additional errors introduced while body outlines
335   are reconstructed around the skeleton. One way to remedy this problem may be to employ the
336   minimum hull approach of Sellers et al. (2012), where the body mass is estimated by multiplying
337   the minimum skeletal hull volume by an empirical ratio between such volumes and the actual
338   volumes in extant mammals. In the present case, the volume of an animal may be estimated from
339   a set of orthogonal minimum skeletal hull silhouettes, provided that the ratio between Paleomass
340   estimates from such silhouettes and the true volume is known. However, derivation of such a
341   ratio would require a broad taxonomic sample of CT scan data that records both the skeletons

342   and body surface of individuals. At present, most publicly available CT scans of marine
343   vertebrates are based on liquid preserved and sometimes eviscerated individuals that do not
344   retain the original body outlines (e.g., MorphoSource.org, Kamminga et al., 2017), making it
345   difficult to obtain sufficient data. This possibility may be pursued in the future as more data are
346   added to public data repositories.
347   At present, it is difficult to assess how much loss of accuracy would result from body
348   outline reconstruction errors based on fossils. However, even if the error level increases by ten-
349   to twenty-fold compared to that from the Paleomass software alone, the total error level would
350   still be comparable to those of other body mass estimation methods for fossil vertebrates. For
351   example, the minimum hull approach had 11-20% errors when applied to primates (Brassey &
352   Sellers, 2014), whereas the mean absolute error is 26.35% in the regression-based body mass
353   estimation of terrestrial vertebrates, with the maximum absolute error being about 300% based
354   on the data in Campione & Evans (2012).
355   Paleomass fills the niche left by other body mass estimation methods. It is applicable to
356   animals for which limb-based regression methods are not suitable, as noted earlier for marine
357   vertebrates. It also enables body mass estimation from flattened fossils, which would supply the
358   body outline images but not a 3D skeletal model necessary for minimum hull construction—
359   again, marine vertebrate fossils tend to be flattened. Application to flattened fossils would
360   depend on the availability of two conspecific individuals with almost identical sizes, exposing
361   the body from two different angles, as in *Stenopterygius* reconstructed by Motani (2001).
362   Overall, Paleomass is a viable alternative to existing body mass estimation methods for fossil
363   vertebrates.

Conclusions

365   Paleomass allows estimation of body volume and surface areas of marine vertebrates with
366   straight body axis through bracketing with 3D models with superelliptical cross-sections. The 3D
367   models are built based on orthogonal silhouettes of the animal in question, which are supplied by
368   the user as raster images. The volumes are converted to body mass by assuming a total body
369   density, which may be the seawater density (1.027 g/cm^3) for forms that use the lungs or air
370   bladders to control buoyancy. Optimal superelliptical values for bracketing are 2.0 and 2.4 for
371   cetaceans, 1.8 and 2.0 for sharks, and 1.8 and 2.1 for most bony fish, although the values may be
372   higher or lower for unusual forms, such as pufferfish and flatfish. When using proper exponent
373   ranges, the errors in volume estimation are about 1.33% on average. The software is open access
374   under GNU General Public License v3.0. at https://github.com/rmotani/paleomass.

Acknowledgements

378 References

379 Anderson JF, Hall-Martin A, Russell DA. 1985. Long-bone circumference and weight in
380   mammals, birds and dinosaurs. *Journal of Zoology* 207:53–61. DOI: 10.1111/j.1469-
381   7998.1985.tb04915.x.
382 Baldridge HD. 1970. Sinking factors and average densities of florida sharks as functions of liver
383   buoyancy. *Copeia* 1970:744–754.
384 Barthelmé S, Tschumperlé D. 2019. imager: an R package for image processing based on CImg.
385   *Journal of Open Source Software* 4:1012. DOI: 10.21105/joss.01012.
386 Brassey CA, Sellers WI. 2014. Scaling of convex hull volume to body mass in modern primates,
387   non-primate mammals and birds. *PLoS ONE* 9. DOI: 10.1371/journal.pone.0091691.
388 Buchner HHF, Savelberg HHCM, Schamhardt HC, Barneveld A. 1997. Inertial properties of
389   Dutch Warmblood horses. *Journal of Biomechanics* 30:653–658. DOI: 10.1016/S0021-
390   9290(97)00005-5.
391 Campione NE, Evans DC. 2012. A universal scaling relationship between body mass and
392   proximal limb bone dimensions in quadrupedal terrestrial tetrapods. *BMC Biology* 10:60.
393   DOI: 10.1186/1741-7007-10-60.
394 Cignoni P, Cignoni P, Callieri M, Callieri M, Corsini M, Corsini M, Dellepiane M, Dellepiane
395   M, Ganovelli F, Ganovelli F, Ranzuglia G, Ranzuglia G. 2008. MeshLab: an open-source
396   mesh processing tool. *Sixth Eurographics Italian Chapter Conference*. DOI:
397   10.2312/LocalChapterEvents/ItalChap/ItalianChapConf2008/129-136.
398 Colbert EH. 1962. The weights of dinosaurs. *American Museum Novitates* 2076:1–16.
399 Dahms WT, Glass AR. 1982. Correlation of percent body fat with body specific gravity in rats.
400   *The Journal of Nutrition* 112:398–400. DOI: 10.1093/jn/112.2.398.
401 Delsett LL, Friis H, Kölbl-Ebert M, Hurum JH. 2022. The soft tissue and skeletal anatomy of
402   two Late Jurassic ichthyosaur specimens from the Solnhofen archipelago. *PeerJ* 10:e13173.
403   DOI: 10.7717/peerj.13173.
404 Gregory WK. 1905. The Weight of the *Brontosaurus*. *Science* 22:572–572. DOI:
405   10.1126/science.22.566.572.a.
406 Hurlburt G. 1999. Comparison of body mass estimation techniques , using recent reptiles and the
407   pelycosaur Edaphosaurus boanerges. *Society* 19:338–350.
408 Irschick DJ, Martin J, Siebert U, Kristensen JH, Madsen PT, Christiansen F. 2021. Creation of
409   accurate 3D models of harbor porpoises (*Phocoena phocoena*) using 3D photogrammetry.
410   *Marine Mammal Science* 37:482–491. DOI: 10.1111/mms.12759.
411 Jerison HJ. 1973. *Evoltuion of the Brain and Intelligence*. New York: Academic Press.
412 Kamminga P, De Bruin PW, Geleijns J, Brazeau MD. 2017. X-ray computed tomography library
413   of shark anatomy and lower jaw surface models. *Scientific Data* 4:1–6. DOI:
414   10.1038/sdata.2017.47.
415 Kano Y, Adnan MS, Grudpan C, Grudpan J, Magtoon W, Musikasinthorn P, Natori Y,
416   Ottomanski S, Praxaysonbath B, Phongsa K, Rangsiruji A, Shibukawa K, Shimatani Y, So
417   N, Suvarnaraksha A, Thach P, Thanh PN, Tran DD, Utsugi K, Yamashita T. 2013. An
418   online database on freshwater fish diversity and distribution in Mainland Southeast Asia.
419   *Ichthyological Research* 60:293–295. DOI: 10.1007/s10228-013-0349-8.
420 Ladson CL, Brooks CW. 1975. Development of a computer program to obtain ordinates for
421   NACA 4-digit, 4-digit modified, 5-digit, and 16-series aerofoils. *NASA Technical
422   Memorandum* X_3284:1–23.

423 Loader C. 1999. Fitting with LOCFIT. *Local Regression and Likelihood*:45–58.
424 Mendoza M, Janis CM, Palmqvist P. 2006. Estimating the body mass of extinct ungulates: a
425   study on the use of multiple regression. *Journal of Zoology* 270:90–101. DOI:
426   10.1111/j.1469-7998.2006.00094.x.
427 Motani R. 2001. Estimating body mass from silhouettes: Testing the assumption of elliptical
428   body cross-sections. *Paleobiology* 27:735–750.
429 Motani R. 2005. Evolution of fish-shaped reptiles (Reptilia : Ichthyopterygia) in their physical
430   environments and constraints. *Annual Review of Earth and Planetary Sciences* 33:395–420.
431   DOI: 10.1146/annurev.earth.33.092203.122707.
432 Murdoch D. 2001. RGL: An R Interface to OpenGL. *Proceedings of the 2nd International
433   Workshop on Distributed Statistical Computing, March 15--17.*
434 R-Core-Team. 2020. *R: A language and environment for statistical computing.* Vienna, Austria:
435   R Foundation for Statistical Computing, Vienna, Austria. URL http://www.R-project.org/.
436 Schlager S. 2017. *Morpho and Rvcg - shape analysis in R: R-packages for geometric
437   morphometrics, shape analysis and surface manipulations*. Elsevier Ltd. DOI:
438   10.1016/B978-0-12-810493-4.00011-0.
439 Schmidt-Nielsen K. 1984. *Scaling: Why is Animal Size so Important?* Cambridge: Cambridge
440   University Press.
441 Seebacher F. 2001. A new method to calculate allometric length-mass relationships of dinosaurs.
442   *Journal of Vertebrate Paleontology* 21:51–60. DOI: 10.1671/0272-
443   4634(2001)021[0051:ANMTCA]2.0.CO;2.
444 Sellers WI, Hepworth-Bell J, Falkingham PL, Bates KT, Brassey CA, Egerton VM, Manning PL.
445   2012. Minimum convex hull mass estimations of complete mounted skeletons. *Biology
446   Letters* 8:842–845. DOI: 10.1098/rsbl.2012.0263.
447 Smith RJ. 2002. Estimation of Body Mass in Paleontology. *Journal of Human Evolution* 43:271–
448   287. DOI: 10.1006/jhev.2002.0573.
449 Soetaert K. 2022. plot3D: Plotting Multi-Dimensional Data. *CRAN website*.
450 Stewart RH. 2008. *Introduction to Physical Oceanography*. Open Textbook Library.

451

452

453

454 Figure 1. How superellipses of different exponent values are used to bracket the true volume of a
455 marine vertebrate. (A) variations of superelliptical shapes, with numbers being the exponents
456 used to produce respective shapes. (B) a skinny dolphin model with an n value of 1.5 based on
457 the silhouettes from D. (C) Same with an exponent of 2.0. (D) 3D model of Tursiops truncates
458 (model 61 from digitallife3d.org). (E) A fat model with an exponent of2.5. (F) Same with an
459 exponent of 3.0.

460

461 Figure 2. Shape input images from *Sphyrna lewini*. (A) Orthogonal views of the target animal,
462 with the overall outlines traced in red. (B) Planar views of fins that are angled in A, with fins in
463 question outlined in red. (C) Input images for Paleomass based on A and B, where fins are
464 separated from the main body. Scale bar in 10cm. A resulting Paleomass mode is found in Fig.
465 4A.

466

467 Figure 3. Computation process of main body and fin/flipper 3D meshes with examples from
468 *Cephalorhynchus heavisidii*. (A) Lateral silhouette image input. (B) Dorso-ventral silhouette
469 image input. (C) Coordinates around A in dots, with dorso-ventral diameters in lines, down-
470 sampled to one in every ten coordinates for visualization purposes. (D) Same as C but based on
471 B. (E) Serial superelliptical sections based on diameters from C and D, with an exponent of 2,
472 downsampled at the same rate as in C. (F) Same as E but with an exponent of 3. (G) 3D mesh
473 combining all superelliptical slices as in E but without downsampling. (H) Same as G but based
474 on F. (I) Same as G but with interpolation with local regression with a nearest neighbor
475 parameter of 0.1. (J) Same as H but with interpolation with local regression. (K) Planar silhouette
476 image input. (L) Coordinates around A in dots, with chords in lines. Downsampled to one in
477 every five slices for visualization purposes. (M) Serial foil section based on NACA 0020,
478 downsampled at the same rate as in L. (N) 3D mesh that connected serial foil sections as in C but
479 without downsampling. (O) Same as C but with interpolation with a nearest neighbor parameter
480 of 0.05. M-O are slightly tilted for visualization purposes and thus appear narrower than K-L.
481
482 Figure 4. Range of body designs modelled by Paleomass. (A) *Sphyrna lewini*. (B) *Rhincodon*
483 *typus*. (C) *Tursiops truncatus*. (D) *Stenopterygius quadriscissus*. (E) *Chaohusaurus*
484 *chaoxianensis*. (F) *Plesiopterys guilelmiimperatoris*. (G) *Latolabrax japonicus. (H) Eopsetta*
485 *grigorjewi. (I) Anguilla marmorata.*
486
487 Figure 5. Errors from volume and surface area estimates for a sphere and prolate spheroid
488 depending on the input image resolution. (A) Errors from the sphere. (B) Errors from a prolate
489 spheroid whose major axis is five times the minor axis. Blue lines are for the surface area and
490 black for the volume. The independent is the number of pixels along the long axis of the
491 geometry, i.e., pixels per diameter.
492
493 Figure 6. Optimal superelliptical exponents for 25 species of extant marine vertebrates, with
494 coronal views of five species. Horizontal bars show the range of optimal superelliptical
495 exponents for individual species. Coronal views are given for the following species. (A)
496 *Mustelus manazo*. (B) *Phocoena phocoena*. (C) *Clupea pallasii*. (D) *Auxis thazad*. (E) *Salvelinus*
497 *leucomaenis*. Species with V-shaped ventral halves of the coronal views, e.g., C, tend to have
498 lower exponent values than those with U-shaped ventral halves, such as E. Squares associated
499 with coronal views are each 1cm.

Figure 1

How superellipses of different exponent values are used to bracket the true volume of a marine vertebrate

(A) variations of superelliptical shapes, with numbers being the exponents used to produce respective shapes. (B) a skinny dolphin model with an n value of 1.5 based on the silhouettes from D. (C) Same with an exponent of 2.0. (D) 3D model of Tursiops truncates (model 61 from digitallife3d.org). (E) A fat model with an exponent of2.5. (F) Same with an exponent of 3.0.
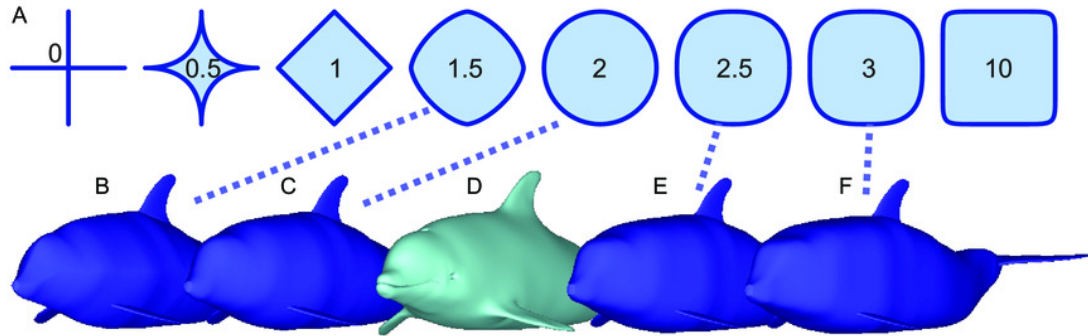
Figure 2

Shape input images from *Sphyrna lewini*

Figure 2. Shape input images from *Sphyrna lewini*. (A) Orthogonal views of the target animal, with the overall outlines traced in red. (B) Planar views of fins that are angled in A, with fins in question outlined in red. (C) Input images for Paleomass based on A and B, where fins are separated from the main body. Scale bar in 10cm. A resulting Paleomass mode is found in Fig. 4A
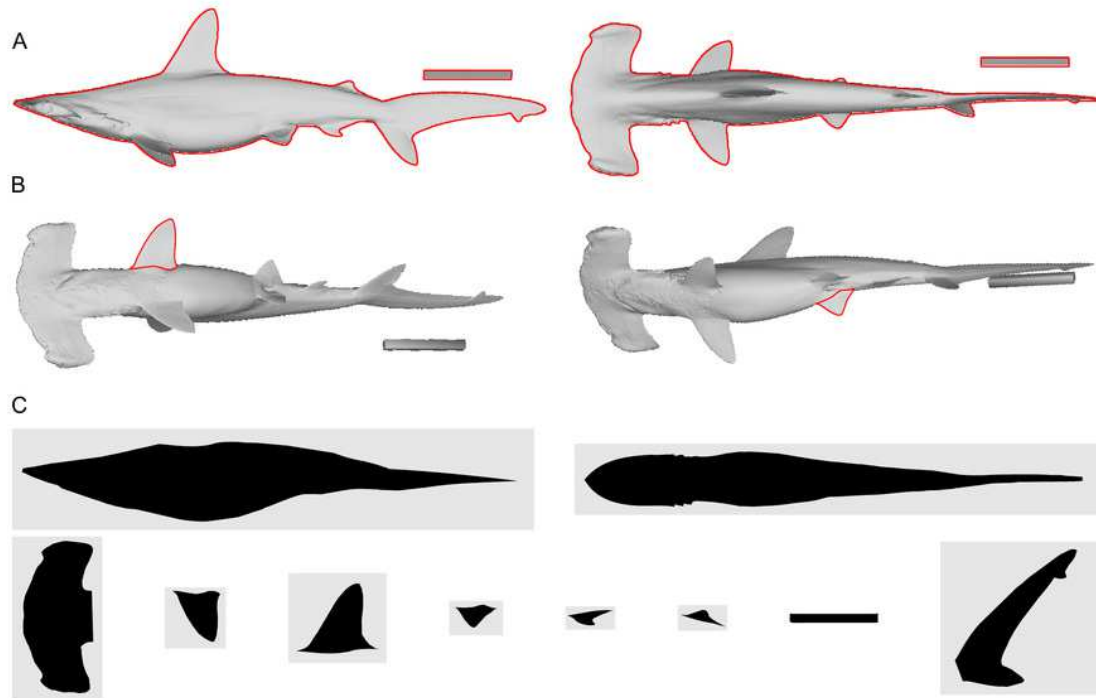
Figure 3

Computation process of main body and fin/flipper 3D meshes with examples from *Cephalorhynchus heavisidii*

(A) Lateral silhouette image input. (B) Dorso-ventral silhouette image input. (C) Coordinates around A in dots, with dorso-ventral diameters in lines, down-sampled to one in every ten coordinates for visualization purposes. (D) Same as C but based on B. (E) Serial superelliptical sections based on diameters from C and D, with an exponent of 2, downsampled at the same rate as in C. (F) Same as E but with an exponent of 3. (G) 3D mesh combining all superelliptical slices as in E but without downsampling. (H) Same as G but based on F. (I) Same as G but with interpolation with local regression with a nearest neighbor parameter of 0.1. (J) Same as H but with interpolation with local regression. (K) Planar silhouette image input. (L) Coordinates around A in dots, with chords in lines. Downsampled to one in every five slices for visualization purposes. (M) Serial foil section based on NACA 0020, downsampled at the same rate as in L. (N) 3D mesh that connected serial foil sections as in C but without downsampling. (O) Same as C but with interpolation with a nearest neighbor parameter of 0.05. M-O are slightly tilted for visualization purposes and thus appear narrower than K-L.
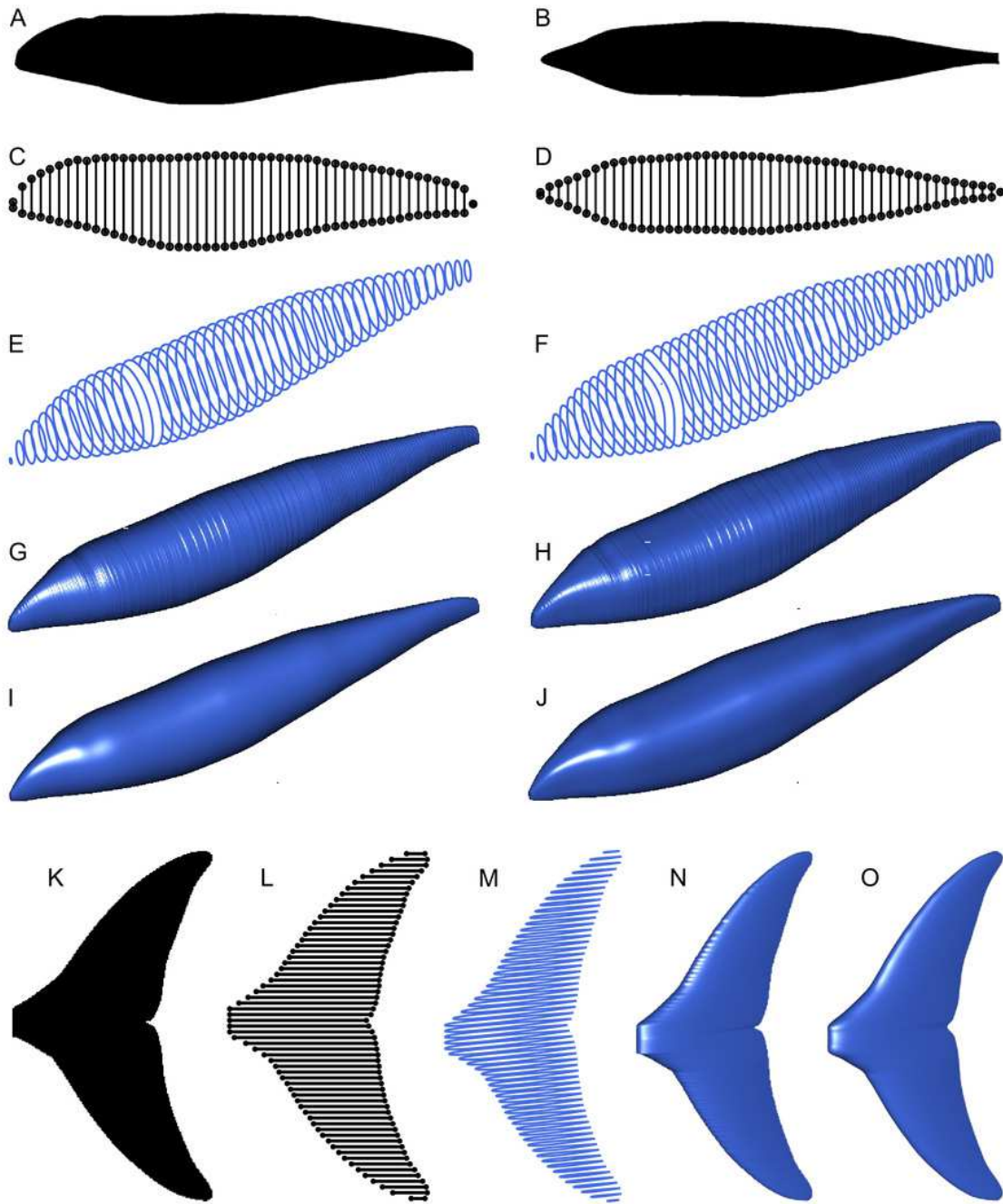
Figure 4

Range of body ~~designs~~ modelled by Paleomass.

(A) *Sphyrna lewini*. (B) *Rhincodon typus*. (C) *Tursiops truncatus*. (D) *Stenopterygius quadriscissus*. (E) *Chaohusaurus chaoxianensis*. (F) *Plesiopterys guilelmiimperatoris.* (G) *Latolabrax japonicus. (H) Eopsetta grigorjewi. (I) Anguilla marmorata.*
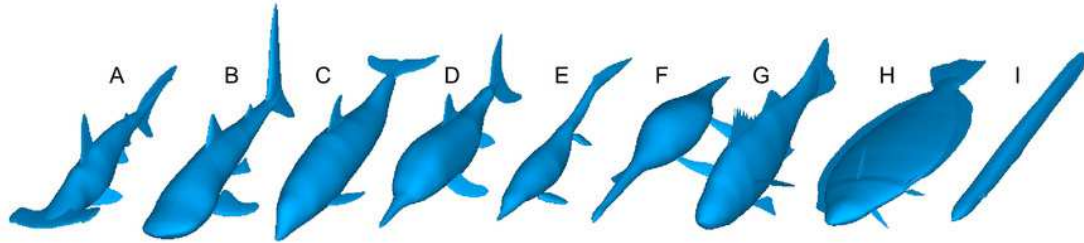
Figure 5

Errors from volume and surface area estimates for a sphere and prolate spheroid depending on the input image resolution.

(A) Errors from the sphere. (B) Errors from a prolate spheroid whose major axis is five times the minor axis. Blue lines are for the surface area and black for the volume. The independent is the number of pixels along the long axis of the geometry, i.e., pixels per diameter.
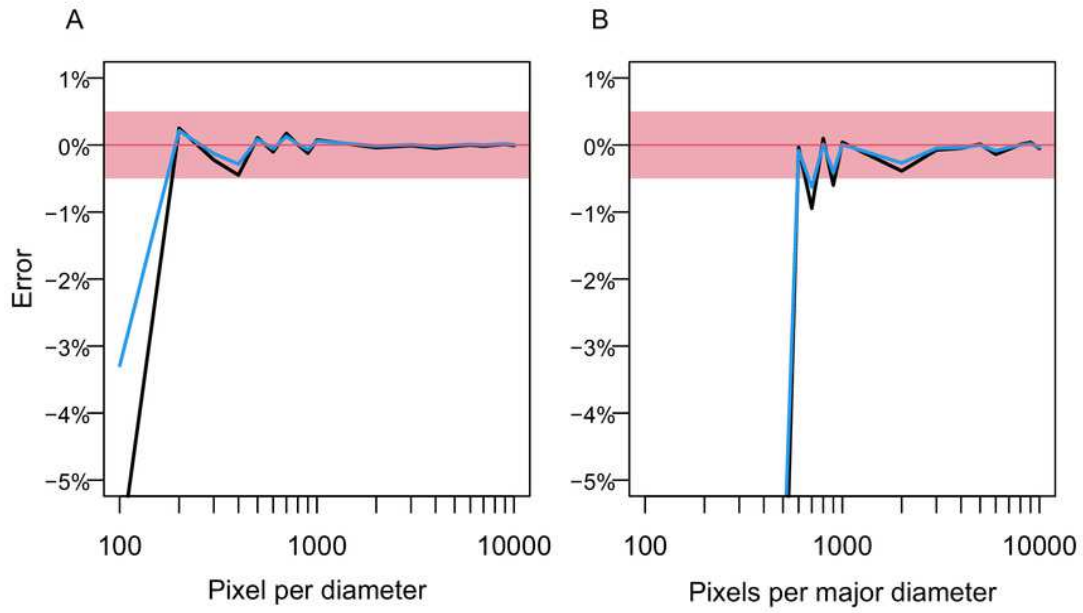
Figure 6

Optimal superelliptical exponents for 25 species of extant marine vertebrates, with coronal views of five species

Horizontal bars indicate the range of optimal superelliptical exponents for individual species. Coronal views are given for the following species. (A) *Mustelus manazo*. (B) *Phocoena phocoena*. (C) *Clupea pallasii*. (D) *Auxis thazad*. (E) *Salvelinus leucomaenis*. Species with V-shaped ventral halves of the coronal views, e.g., C, tend to have lower exponent values than those with U-shaped ventral halves, such as E. Squares associated with coronal views are each 1cm.